J. Phys. B: At. Mol. Opt. Phys. **22** (1989) 531-540. Printed in the UK

Experimental cross sections for electron impact ionisation of hydrogen-like Li^{2+} ions

K Tinschert†‖, A Müller†, G Hofmann†, K Huber†, R Becker‡, D C Gregory§ and E Salzborn†

† Institut für Kernphysik, Universität Giessen, D-6300 Giessen, Federal Republic of Germany

‡ Institut für Angewandte Physik, Universität Frankfurt, D-6000 Frankfurt, Federal Republic of Germany

§ Physics Division, Oak Ridge National Laboratory, Oak Ridge, Tennessee 37831-6372, USA

Received 1 August 1988

Abstract. Absolute measurements have been made of cross sections for the ionisation of Li^{2+} ions by electrons with energies which range from threshold (122.45 eV) to 1000 eV. The results are in good agreement with available distorted-wave exchange calculations. The scaling behaviour of ionisation cross sections along the hydrogen isoelectronic sequence is discussed.

1. Introduction

Ionisation of hydrogen-like systems by electron impact is among the most fundamental collision processes. With only one electron that can be removed the H-like systems are the simplest targets to be used in ionisation studies. Nevertheless, the free motion of three particles within their mutual potential cannot be properly represented, and hence ionisation theory is never fundamentally satisfying.

Experiments on H-like systems are not straightforward either. Preparation and experimental control of the target require substantial efforts and the resulting intensity problems make measurements time-consuming and tedious. Although the phenomenon of electron impact ionisation of atoms has been studied since about 100 years ago, it was not until 1958 that the first (relative) measurements of ionisation cross sections for atomic hydrogen were reported (Fite and Brackmann 1958). In 1961 the first electron–ion crossed-beams experiment followed, yielding absolute cross sections for the ionisation of He^{1+} ions (Dolder *et al* 1961). Progress was achieved later by doing more accurate measurements of total cross sections (Rothe *et al* 1962, McGowan and Clarke 1968, Defrance *et al* 1981a, Shah *et al* 1987), by including metastable hydrogen (Dixon *et al* 1975, Defrance *et al* 1981b) and by doing sophisticated triply differential measurements on atomic hydrogen in its ground state (Ehrhardt *et al* 1986). New data on multiply charged ions up to Ar^{17+} were obtained by modelling the charge-state evolution of ions in a trap (Donets and Ovsyannikov 1980). However, He^{+} remained the only H-like ion studied in direct crossed-beams measurements.

On the theory side, considerable progress was made (Rudge and Schwartz 1966, Younger 1980, 1981, Byron *et al* 1983, 1984, Joachain *et al* 1985) and the advanced

‖ This work contains parts of K Tinschert's thesis, Giessen D26.

0953-4075/89/030531+10$02.50

calculations of total ionisation cross sections for hydrogen-like systems are in very good agreement with the available experiments. It has been reasoned 'that the theory for these cases proves that the experiments are basically correct rather than the other way around' (Crandall 1983). Since the more stringent tests for theory by differential measurements on electron impact ionisation of ions are presently not possible because of intensity problems and because of the relative difficulty even to go only one more charge state up in the hydrogen-like isoelectronic sequence, nobody has so far attempted to do crossed-beams measurements of total ionisation cross sections for Li^{2+} ions or beyond.

Both as a test of our experimental technique and as a test of the available theory we have measured absolute electron impact ionisation cross sections for Li^{2+} ions in the energy range from threshold up to 1000 eV. We compare our data with measurements on H atoms and He^{+} ions using the theoretical scaling laws and give an outlook on the situation for very highly charged members of the hydrogen-like isoelectronic sequence.

2. Experimental technique

Extensive reports on the techniques of experiments with crossed electron and ion beams are available, and many details of our apparatus and associated uncertainties have been published (Müller *et al* 1985a, Tinschert *et al* 1987). However, recent changes of the experimental set-up require some discussion. Figure 1 shows a schematic view of the apparatus. Ions are produced by an electron-cyclotron-resonance (ECR) ion

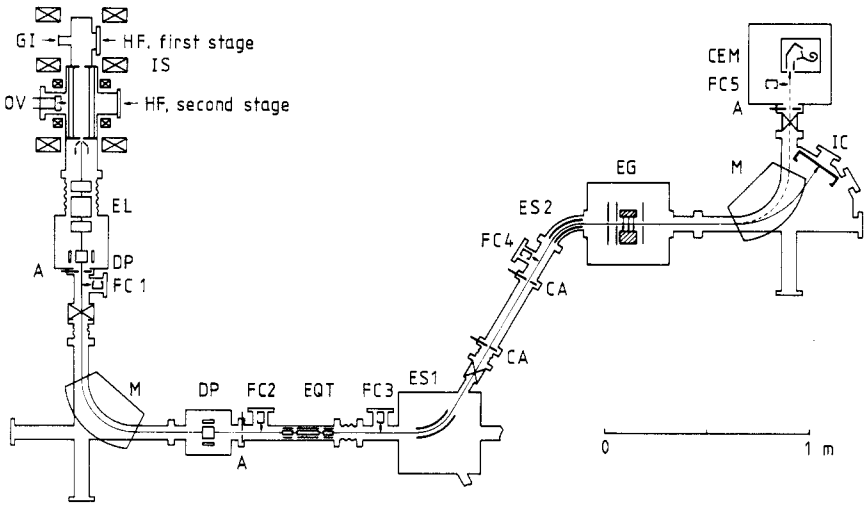

Figure 1. Schematic view of the experimental set-up, including the whole beamline from the ion source to the detector for ionised ions: IS, ECR ion source with gas inlet (GI), microwave power inlet (HF) into the first and second stages of the ion source and a directly heated oven (OV) for evaporation of metallic lithium; EL, einzel lens; DP, pairs of electrostatic deflection plates; A, variable apertures; FC1, ..., FC5, movable Faraday cups; M, 90° analysing magnets; EQT, electrostatic quadrupole triplet; ES1 and ES2, 60° spherical condensers; CA, collimating apertures; EG, high-power electron gun with selectable ion beam apertures; IC, large Faraday cup collecting the parent ion beam; CEM, channel-electron-multiplier-based single-particle detector for the ionised product ions.

source (Mank *et al* 1986), formed into a beam and then momentum-analysed by a magnet. By electrostatic focusing and deflection elements the desired ion beam is transported through a collimation system to the interaction region. Ionisation products and the parent ion beam are separated by a second magnet. The incident ions are collected by a wide Faraday cup inside the magnet chamber and the ionised ions are simultaneously detected by a channel-electron-multiplier-based single-particle detector (Rinn *et al* 1982).

For the measurement of an absolute cross section we use the technique described by Müller *et al* (1985b). The electron beam is moved up and down across the ion beam. At each of about 500 intermediate positions characterised by intervals $\Delta Z = 0.036$ mm we measure and store simultaneously the number of ionised ions and accumulated electron and ion charges. For this purpose the electrical currents are converted to proportional frequencies. The dwell time for one half period of the electron gun movement per interval ΔZ corresponding to one channel in a multichannel analyser (MCA) spectrum is about 0.1 s. After a number of movements we divide the number of accumulated signal counts from each channel in the signal spectrum by the contents of the corresponding channel in the ion-beam-current spectrum. In the region where both beams overlap and ionisation is possible the signal spectrum and also the divided spectrum show a peak. The peak content S in the divided spectrum is directly proportional to the measured cross section σ

$$\sigma = \frac{S\Delta Z}{MI_e\varepsilon} K. \tag{1}$$

The constant K contains the conversion factors of integrated beam currents into numbers of counts, I_e is the electron current, ε is the detector efficiency and M is a kinematic factor given by

$$M = (v_e^2 + v_i^2)^{1/2}/(v_e v_i q e^2). \tag{2}$$

Here v_e is the electron velocity, v_i the ion velocity, q the parent-ion charge state and e the charge of an electron.

2.1. Ion-beam preparation

The two-stage ECR ion source (see figure 1) is operated with a microwave frequency of 5 GHz. From a small oven with a 3 mm diameter aperture metallic lithium is evaporated into the second stage. Positive ions are accelerated by a static source potential of +10 kV and then focused (see figures 1 and 2) by an einzel lens to the entrance aperture of a double-focusing 90° magnet. The height of the magnet chamber inside the gap is 32 mm, which limits the emittance of the ion beam to some extent. At the 1:1 image point a movable Faraday cup serves to measure charge-state-analysed ion currents. The electrical current of $^7Li^{2+}$ ions obtained at this position was of order 5 μA. Between the first magnet and the interaction chamber only electrostatic optical elements are used so that it is possible to sweep the first magnet and leave the down-beam ion optics unchanged. This provides a handy tool for beam purity diagnostics. The beam line up to the interaction chamber provides a mass/charge resolution which is greater than 300.

Optical elements are an electrostatic quadrupole triplet, a 60° spherical deflector, two collimating apertures, a second 60° spherical deflector and two more collimating apertures just in front of the intersection with the electron beam. The Li^{2+} ion beam

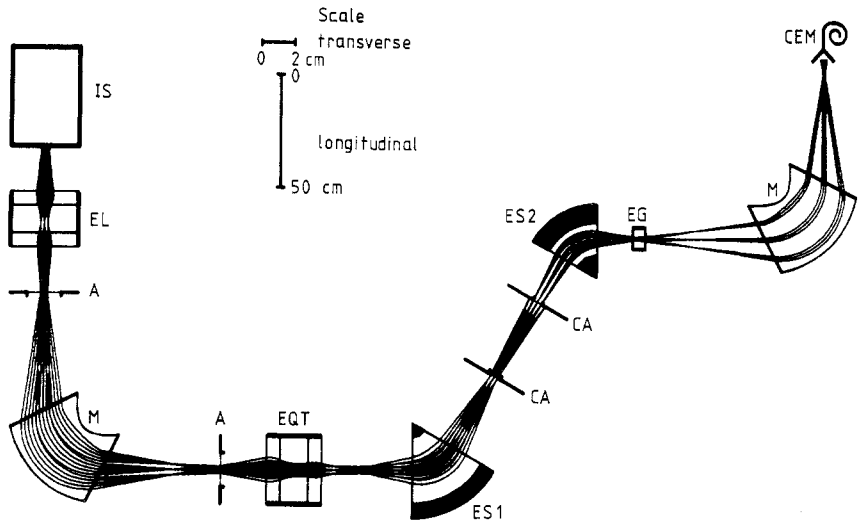

Figure 2. Computer simulation of ion beam trajectories in the beam transport system shown in figure 1 using the GIOS ion optics calculation program (Wollnik *et al* 1987): IS, ion source; EL, einzel lens; A, variable apertures; M, double-focusing analysing magnets (90° deflection angle, 250 mm deflection radius); EQT, electrostatic quadrupole triplet; ES1, electrostatic spherical condenser (200 mm deflection radius); CA, collimating apertures; ES2, electrostatic spherical condenser (170 mm deflection radius); EG, electron gun; CEM, single-particle detector.

is cut to below 1 mm diameter and its current is typically reduced to the level of 1% of the original value.

The second magnet is identical to the first magnet and is set to form a 1:1 image of the beam interaction region onto an iris aperture in front of the single-particle detector for the ionised ions. An aperture setting of 7 mm diameter was shown to guarantee collection of all product ions.

The parent ion beam is collected in a wide Faraday cup inside the magnet chamber. Ratios of initial and final ion charges between $\frac{8}{9}$ and $\frac{1}{4}$ can be accommodated without changing the position of the cup, i.e. triple ionisation of a singly charged ion as well as single ionisation of an ion with charge state 8 can be measured by controlling parent and product beams simultaneously.

Differential pumping in the beam line reduces the pressure from the operating pressure of the ion source, about 5×10^{-6} mbar, to approximately 5×10^{-10} mbar in the collision chamber with both beams on (electron current below 10 mA). During the measurements we flood the collision chamber with Kr gas at a pressure of typically 1×10^{-7} mbar. We have shown earlier that this pressure is sufficient to neutralise the space charge of the electrons in the gun and to allow accurate cross section measurements (Müller *et al* 1987). Test measurements below ionisation thresholds are used to control whether there is an influence from collisions of ions in the parent beam with Kr ions trapped in the electron beam.

2.2. Electron gun

The present version of our electron gun and measurements of its properties were described before (Müller *et al* 1985a, 1987, Becker *et al* 1985). Space-charge-limited

electron-beam currents of up to 460 mA at 1 keV are obtained. The beam is 60 mm wide and about 2 mm high at 1 keV, providing a current density of nearly 0.4 A cm^{-2} and a spatial density of about 10^9 cm^{-3}. The potentials applied to the gun electrodes and the space charge of the electrons create a three-dimensional ion trap with cylindrical symmetry along the ion beam axis. The calculated total depth of the potential well is 4% of the electron energy with a near-parabolic radial dependence. The electron energy spread resulting from such a potential distribution would be expected to be 4 eV at an energy of 100 eV. However, there are trapped ions compensating the electron space charge. In recent measurements we found very narrow dielectronic capture resonances with subsequent multiple electron emission in electron impact ionisation of heavy ions of Xe, Cs, Ba, La and Ce (Müller *et al* 1988). Widths of less than 0.4 eV were observed for about 100 eV electron energy, setting a rather low upper limit to the energy spread in the electron beam.

3. Results

The cross sections measured for electron impact ionisation of Li^{2+} ions are given in table 1 together with their statistical uncertainties (90% confidence level). The quadrature sum of non-statistical errors is 7.8% resulting from uncertainties in the detection efficiency (0.97 ± 0.03), the channel width ($\pm 1\%$), the ion and electron currents ($\pm 5\%$) as well as ion and electron velocities ($\pm 1\%$). The total uncertainty is typically $\pm 10\%$ at maximum.

Table 1. Measured cross sections $\sigma_{2,3}$ for electron impact ionisation of Li^{2+} ions. The statistical uncertainties are given at 90% confidence level.

Electron energy (eV)	Cross section (10^{-19} cm^2)	Electron energy (eV)	Cross section (10^{-19} cm^2)
120.0	0.56 ± 0.71	350.0	10.1 ± 0.5
124.0	0.66 ± 0.67	400.0	10.4 ± 0.5
135.0	2.35 ± 0.50	450.0	10.2 ± 0.5
150.0	3.77 ± 0.63	520.0	9.66 ± 0.39
165.0	5.03 ± 0.72	600.0	9.63 ± 0.40
180.0	6.09 ± 0.63	650.0	9.27 ± 0.32
200.0	7.76 ± 0.54	720.0	8.63 ± 0.34
220.0	7.64 ± 1.04	850.0	8.40 ± 0.37
260.0	8.82 ± 0.51	1000.0	7.48 ± 0.25
300.0	9.56 ± 0.33		

4. Discussion

Our results are displayed in figure 3. Total uncertainties are indicated. Also shown are cross sections calculated from the three-parameter Lotz formula (Lotz 1968) and the distorted-wave exchange approximation (Younger 1980, 1981). Theory and experiment nicely support each other. Indeed there seems to be no problem nowadays to predict total electron impact ionisation cross sections for hydrogenic ions.

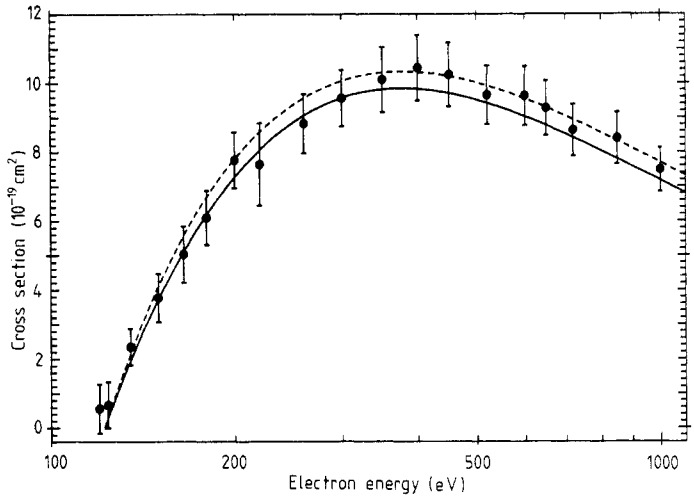

Figure 3. Cross section for electron impact ionisation of Li^{2+} ions: ●, present measurements (error bars indicate the total experimental error including the statistical error at 90% confidence level); ——, distorted-wave exchange (DWX) calculation of Younger (1981); - - -, semi-empirical Lotz formula (Lotz 1968).

The basic scaling rule for ionisation cross sections σ of hydrogen-like systems was already found by Thomson (1912)

$$\sigma I^2 = f(E/I). \tag{3}$$

A general function f depending only on the ratio E/I of projectile electron energy E and target electron binding energy I results when σ is multiplied by I^2. This is not exactly true for low atomic numbers Z because of the transition from a screened ion nucleus for $Z = 1$ to a charged target with a long-range Coulomb field for $Z \geq 2$. With increasing Z, equation (3) was predicted to give an increasingly better description of reality. Figure 4 displays the scaled cross sections σI^2 versus E/I for all measurements done on ground-state hydrogenic systems so far. The scaling appears to work quite well. All data points are grouped around a hypothetical universal curve. A closer look at the data shows, however, that for low ratios E/I the cross sections increase with Z. The reason for this is the change of screening discussed above which has the highest influence at low electron energies. This effect, though somewhat less pronounced, is also seen in the theoretical cross section curves calculated by Rudge and Schwartz (1966) for $Z = 1$, $Z = 2$ and $Z = 128$ which are also displayed in figure 4.

Only for $Z = 1$ does the theory overestimate the experimental results, but for $Z = 2$ there is almost perfect agreement between experiment and theory. The full curve represents the theoretical cross section calculation of Moores *et al* (1980) for the $Z = \infty$ limit, the maximum of which coincides with the $Z = 128$ result of Rudge and Schwartz (1966). Minor discrepancies between theories at high ratios of E/I where the Bethe limit is nearly reached are probably due to the special choice of parameters in scaling functions f fitting a limited number of theoretical points. For $Z = 1$ and $Z = 2$ we calculated fit parameters from the calculated cross section values of Rudge and Schwartz. For $Z = 128$ and $Z = \infty$ we used parameters given by the authors of respective theoretical papers.

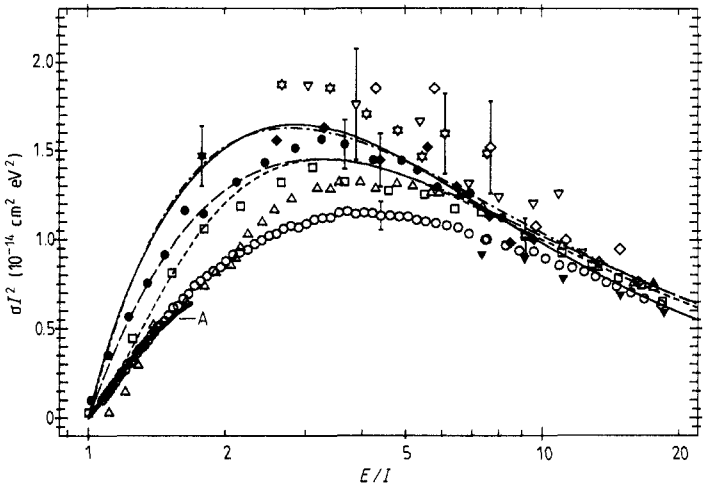

Figure 4. Classically scaled cross sections σI^2 for electron impact ionisation of the H atom and H-like ions plotted against scaled energy E/I (I is the respective ionisation potential).

Experimental results for atomic hydrogen H(1s): thick full curve A, McGowan and Clarke (1968); △, Fite and Brackmann (1958); ▼, Rothe *et al* (1962); ○, Shah *et al* (1987).

Experimental results for hydrogen-like ions: □, cross sections for He^+ (Peart *et al* 1969); ●, cross sections for Li^{2+} (present measurements); ◇, cross sections for C^{5+}; ▽, cross sections for N^{6+}; ◆, cross sections for O^{7+}; open star, cross sections for Ne^{9+}; full star, cross section for Ar^{17+} (Donets and Ovsyannikov 1980, ion-trap measurements). Error bars indicate total experimental errors; only for the results of Donets and Ovsyannikov do the error bars represent the statistical uncertainties.

Theory: Coulomb-Born exchange calculations of Rudge and Schwartz (1966) for $Z = 1$ (short broken curve), $Z = 2$ (long broken curve) and $Z = 128$ (chain curve). We have fitted the results of Rudge and Schwartz with a formula given by the authors for $Z = 1$ and $Z = 2$ in order to represent the results of their calculation as a smooth curve. The full curve shows the calculation of Moores *et al* (1980) for the $Z = \infty$ limit.

Figure 5 presents a collection of the most complete experimental data sets obtained so far for H, He^+ and Li^{2+}. The effect of increasing atomic number and ion charge state on the cross section shape becomes clearly visible. For sufficiently high ratios E/I all three data sets are merged by the scaling into a common functional dependence which is already predicted by the first-order Born approximation. In fact, measurements on the ionisation of atomic hydrogen are sometimes calibrated against the Born or Bethe cross sections at high electron energies. This is not the case for the He^+ and Li^{2+} data which were measured independently absolute. Comparison with the Lotz formula proves once again how well this scaling rule works for electron impact direct ionisation.

The above discussions all lead to a consistent view of ionisation processes of hydrogen-like ions. So, further experiments with higher atomic number would seem like a waste of effort. We want to point out, however, that dramatic changes will occur in figure 4 when the atomic number increases to $Z = 50$ or even to $Z = 92$.

From Bohr's atomic model the electron binding energy for a hydrogen-like atom is $I = 13.6\ \text{eV} \times Z^2$. For $Z = 92$ this would result in $I = 115$ keV and in orbital velocities of the order of $2 \times 10^8\ \text{m s}^{-1}$, suggesting relativistic effects both on the bound electron and the projectile electron which needs relativistic velocities to remove the bound electron. In fact the calculated binding energy of an U^{91+} ion is $I = 131.8$ keV (Johnson

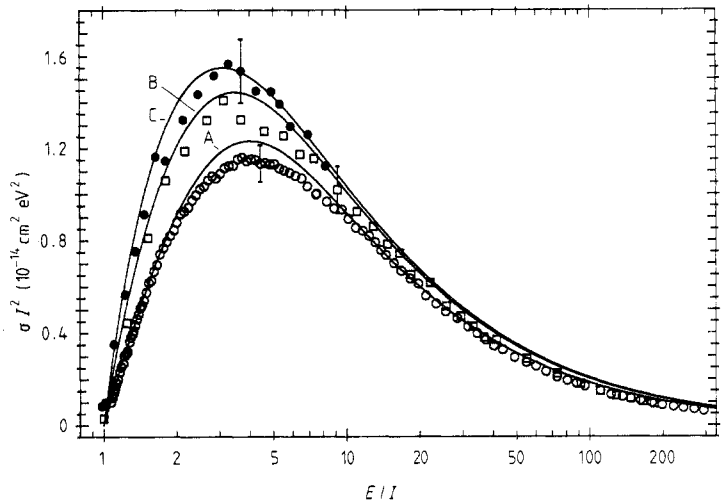

Figure 5. Scaled cross sections for electron impact ionisation of H (Shah *et al* 1987; ○), He^+ (Peart *et al* 1969; □) and Li^{2+} (present measurements; ●) as in figure 4. Error bars indicate total experimental uncertainties. Full curves show the predictions of the semi-empirical Lotz formula (Lotz 1968) for $Z=1$ (curve A), $Z=2$ (curve B) and $Z=3$ (curve C).

and Soff 1985). Owing to the relativistic energy of the ionising electron one has to expect that the scaling of equation (3) fails. Thus the calculations for $Z=128$ and $Z=\infty$ shown in figure 4 are fictitious in two ways: there is no atom with such atomic numbers and if it did exist, its cross section for electron impact ionisation would look completely different from the non-relativistic calculation. For a guess of relativistic effects on ionisation cross sections one could start, for example, from the Lotz formula, which agrees so well with the experiments for low-Z ions and introduce a relativistic correction. Such a correction factor was calculated by Gryzinski (1965) using classical methods. The result was successfully applied to inner-shell ionisation phenomena by Pessa and Newell (1971) and Quarles (1976). The factor is

$$R=\left(\frac{\tau+2}{\varepsilon+2}\right)\left(\frac{\varepsilon+1}{\tau+1}\right)^2\left(\frac{(\tau+\varepsilon)(\varepsilon+2)(\tau+1)^2}{\varepsilon(\varepsilon+2)(\tau+1)^2+\tau(\tau+2)}\right)^{3/2} \tag{4}$$

where $\varepsilon=E/(m_0c^2)$ and $\tau=I/(m_0c^2)$ are the projectile electron energy and the target binding energy, respectively, in electron rest energy units. For $Z\geqslant 3$ the ionisation cross section can be written in the form

$$\sigma=4.5\times10^{-14}\frac{R}{EI}\ln(E/I)\ \text{cm}^2\,\text{eV}^2. \tag{5}$$

In figure 6 we compare this formula for six different values of Z ($Z=3$, 10, 30, 50, 70, 92) with the fictitious calculation for $Z=128$ by Rudge and Schwartz (1966). Obviously for U^{91+} there are considerable differences from the scaling expected on the basis of equation (3) already at electron energies twice the threshold energy. At $E/I=10$ the relativistic cross section calculation exceeds the non-relativistic theory by more than a factor of 5. Although equation (5) was composed only from Lotz's semi-empirical formula and a classical correction factor for relativistic effects it did

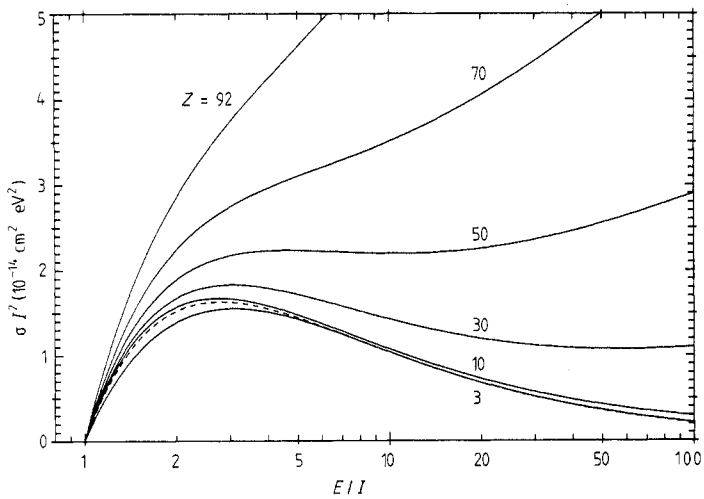

Figure 6. Calculated scaled cross sections for electron impact ionisation of hydrogen-like ions plotted against E/I. Full curves show the results of the Lotz formula (Lotz 1968) multiplied by a relativistic correction factor (Pessa and Newell 1971, Quarles 1976) as described in the text for atomic numbers $Z = 3$, 10, 30, 50, 70 and 92. The broken curve is the calculation for $Z = 128$ of Rudge and Schwartz (1966) without any relativistic correction.

successfully describe inner-shell ionisation cross sections for a wide range of atomic numbers and scaled energies E/I between 1 and 10^5 (Quarles 1976). Hence we believe that our predictions for the hydrogenic ions shown in figure 6 are qualitatively correct.

5. Conclusions

We have performed crossed-beams absolute measurements of electron impact ionisation cross sections for hydrogen-like Li^{2+} ions. These measurements extend the available database for H and He^+ to include a multiply charged ion. While all the available experimental data on total ionisation are in agreement with advanced theoretical calculations we point out considerable changes of scaling behaviour at relativistic energies where a naive interpretation of the available theoretical results would lead to false expectations. These considerations may become immediately relevant when hydrogen-like U^{91+} ions will be stored in a storage ring with electron-beam cooling. A ring which is designed to store completely stripped ions of all elements up to uranium is presently under construction at GSI, Darmstadt.

Acknowledgments

We thank B Weissbecker for his help in preparing the figures. We acknowledge NATO Collaborative Research Grant RG 86/0510, which made the collaboration with DCG possible. This work was supported by Deutsche Forschungsgemeinschaft (DFG), Bonn Bad-Godesberg, and Max-Planck Institut für Plasmaphysik, Garching.

References

Becker R, Müller A, Achenbach C, Tinschert K and Salzborn E 1985 *Nucl. Instrum. Meth.* B **9** 385-8

Byron F W Jr, Joachain C J and Piraux B 1983 *Phys. Lett.* **99A** 427-31

—— 1984 *Phys. Lett.* **106A** 299-300

Crandall D H 1983 *Atomic Physics of Highly Ionized Atoms* ed R Marrus (New York: Plenum)

Defrance P, Brouillard F, Claeys W and Van Wassenhove G 1981a *J. Phys. B: At. Mol. Phys.* **14** 103-10

Defrance P, Claeys W, Cornet A and Poulaert G 1981b *J. Phys. B: At. Mol. Phys.* **14** 111-17

Dixon A J, von Engel A and Harrison M F A 1975 *Proc. R. Soc. Lond.* A **343** 333-49

Dolder K T, Harrison M F A and Thonemann P C 1961 *Proc. R. Soc.* A **264** 367-78

Donets E D and Ovsyannikov V P 1980 *Report* P7-80-404, Joint Institute for Nuclear Research, Dubna, USSR (translation ORNL-tr-4702, available from Technical Information Center, PO Box 62, Oak Ridge, TN 37830, USA)

Ehrhardt H, Jung K, Knoth G and Schlemmer P 1986 *Z. Phys.* D 1 3-32

Fite W L and Brackmann R T 1958 *Phys. Rev.* **112** 1141-51

Gryzinski M 1965 *Phys. Rev.* **138** A336-58

Joachain C J, Piraux B, Potvliege R M, Furtado F and Byron F W Jr 1985 *Phys. Lett.* **112A** 138-40

Johnson W R and Soff G 1985 *At. Data Nucl. Data Tables* **33** 405-46

Lotz W 1968 *Z. Phys.* **216** 241-7

McGowan J W and Clarke E M 1968 *Phys. Rev.* **167** 43-51

Mank G, Liehr M and Salzborn E 1986 *7th Workshop on Electron Cyclotron Resonance (ECR) Ion Sources* Contributed Papers, ed H Beuscher, Berichte der Kernforschungsanlage Jülich—No Jül-Conf-57, Jülich (available from Zentralbibliothek der Kernforschungsanlage Jülich GmbH, Postfach 1913, D-5170 Jülich, FRG) pp 203-14

Moores D L, Golden L B and Sampson D H 1980 *J. Phys. B: At. Mol. Phys.* **13** 385-95

Müller A, Hofmann G, Tinschert K, Sauer R, Salzborn E and Becker R 1987 *Nucl. Instrum. Meth.* B **24/25** 369-72

Müller A, Huber K, Tinschert K, Becker R and Salzborn E 1985a *J. Phys. B: At. Mol. Phys.* **18** 2993-3009

Müller A, Tinschert K, Achenbach C, Salzborn E and Becker R 1985b *Nucl. Instrum. Meth.* B **10/11** 204-6

Müller A, Tinschert K, Hofmann G, Salzborn E and Dunn G H 1988 *Phys. Rev. Lett.* **61** 70-3

Peart B, Walton D S and Dolder K T 1969 *J. Phys. B: At. Mol. Phys.* **2** 1347-52

Pessa V M and Newell W R 1971 *Phys. Scr.* **3** 165-8

Quarles C A 1976 *Phys. Rev.* A **13** 1278-80

Rinn K, Müller A, Eichenauer H and Salzborn E 1982 *Rev. Sci. Instrum.* **53** 829-37

Rothe E W, Marino L L, Neynaber R H and Trujillo S M 1962 *Phys. Rev.* **125** 582-3

Rudge M R H and Schwartz S B 1966 *Proc. Phys. Soc.* **88** 563-78

Shah M B, Elliot D S and Gilbody H B 1987 *J. Phys. B: At. Mol. Phys.* **20** 3501-14

Thomson J J 1912 *Phil. Mag.* **23** 449-57

Tinschert K, Müller A, Hofmann G, Achenbach C, Becker R and Salzborn E 1987 *J. Phys. B: At. Mol. Phys.* **20** 1121-34

Wollnik H, Brezina J and Berz M 1987 *Nucl. Instrum. Meth.* A **258** 408-11

Younger S M 1980 *Phys. Rev.* A **22** 111-17

—— 1981 *J. Quant. Spectrosc. Radiat. Transfer* **26** 329-37